Sensor Fusion for Predicting Vehicles' Path for Collision Avoidance Systems

Aris Polychronopoulos, *Member, IEEE*, Manolis Tsogas, Angelos J. Amditis, *Member, IEEE*, and Luisa Andreone

***Abstract*—Path prediction is the only way that an active safety system can predict a driver's intention. In this paper, a model-based description of the traffic environment is presented—both vehicles and infrastructure—in order to provide, in real time, sufficient information for an accurate prediction of the ego-vehicle's path. The proposed approach is a hierarchical-structured algorithm that fuses traffic environment data with car dynamics in order to accurately predict the trajectory of the ego-vehicle, allowing the active safety system to inform, warn the driver, or intervene when critical situations occur. The algorithms are tested with real data, under normal conditions, for collision warning (CW) and vision-enhancement applications. The results clearly show that this approach allows a dynamic situation and threat assessment and can enhance the capabilities of adaptive cruise control and CW functions by reducing the false alarm rate.**

***Index Terms*—Collision warning (CW), curvilinear motion model, Kalman, path prediction, sensor fusion.**

I. Introduction

AN ADAPTIVE cruise control (ACC) system, which maintains the distance from the preceding vehicle, is available on the market, while the development of next-generation ACC and obstacle avoidance systems is in progress. These systems have to take some action: warn the driver by visual, haptic, or audio signals or intervene, depending on the application. Moreover, forward collision warning (FCW) systems do not consider only the preceding vehicle but also the potential dangers in the adjacent lanes. In such systems, it has identified the necessity to have a reliable path prediction of the ego-vehicle due to the fact that this is the only way to be predictive about the possible driver's intention. In turn, the in-path obstacles should correctly be assigned for use in threat assessment and decision-making functions, minimizing the false alarms of the system.

The conventional warning systems in the market calculate the path based only on on-board sensors (e.g., the yaw rate and the speed value) and a-β filters to reduce the measurement noise. However, estimation of vehicle trajectory, based on current vehicle motion alone, is not sufficient to ensure a correct assignment of the objects which lie on the vehicle's path, leading to a system which is not false-alarm free and not even miss-alarm free (an example of false alarm could be picking up the metal guard rail on a curved road). The reason is twofold. On one hand, the vehicle tends to follow the road geometry. The driver continuously acts on the steering wheel with small adjustments, e.g., when driving straight or following a road with a constant curvature; this produces small effects in the lateral distance of the vehicle from the road center, but the effect on the momentary vehicle curvature radius is significant if extrapolated at a distance. On the other hand, the road geometry evolutes in time, and this should be detected by the sensor system.

Consequently, there has been much effort spent to estimate the road geometry—borders and lanes—for next-generation ACC systems using a single sensor or information fusion techniques. The most common method is based on lane trackers using monocular video sensors that can detect the lanes up to 50 m ahead (e.g., see [1]); in more recent publications, a laser scanner [2], a high-resolution radar [3], and even an infrared camera [4] are also utilized. More efficient approaches propose information fusion techniques to complement the yaw-rate-based road geometry estimate and predict changes in the curvature of the road ahead using a digital map and a GPS receiver, forward looking video cameras, and tracks from the radar or stationary obstacles that represent guardrails or posts [5], [6]. Results of these road geometry estimates are combined by the data fusion function to produce the best estimate of the road geometry ahead of the vehicle. The road geometry estimate that is produced by the fusion function is used by the target selection process to determine which objects that are detected by the radar are in the path of the vehicle.

The aforementioned approach is recommended for ACC functions, but it ignores possible maneuver either of the ego-vehicle or the moving obstacles. For example, what happens if the ego-vehicle is overtaking or carries out a lane change? Neither approach is adequate to model the path as the vehicle initially follows its dynamics for some few seconds and then follows the geometry to switch again if the driver completes a full overtaking maneuver. A high false alarm rate is an obvious consequence when the assigned "dangerous" vehicle in path is changing lane or exits the road. The need of a multiple model approach is therefore promoted, which is accompanied with detection of the maneuvers. Moreover, time factor is also ignored since the geometry is tracked as a line in the vehicle coordinate system; thus, the system produces warnings based only on time to collision and headway in a given time instant.

Manuscript received November 7, 2005; revised August 2, 2006, May 15, 2007, and May 20, 2007. This work was supported in part by the European Commission under the project EUCLIDE, which ended in May 2004. The Associate Editor for this paper was C. Stiller.

A. Polychronopoulos, M. Tsogas, and A. J. Amditis are with the Institute of Communications and Computer Systems, National Technical University of Athens, 15773 Athens, Greece (e-mail: arisp@iccs.gr; mtsog@iccs.gr; a.amditis@iccs.gr).

L. Andreone is with the Fiat Research Centre, 10043 Torino, Italy (e-mail: Luisa.andreone@crf.it).

Color versions of one or more of the figures in this paper are available online at http://ieeexplore.ieee.org.

Digital Object Identifier 10.1109/TITS.2007.903439

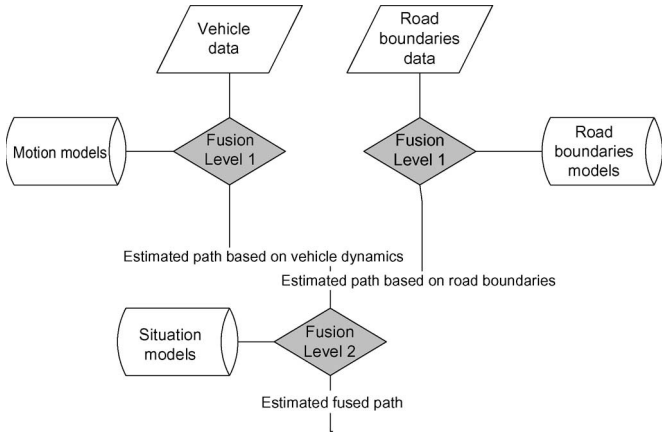

Fig. 1. Structure of the fusion process for the estimation of the ego-path.

Last but not the least, even if the path was based on vehicle dynamics, it would be erroneous to use the conventional circle model since a vehicle may be, at least, in two different modes: maneuvering and nonmaneuvering mode (straight line motion) [7]. A simple example is when a vehicle is slightly accelerating in a curve, which cannot be modeled the same way as when it is moving with a constant velocity.

This paper addresses the aforementioned drawbacks of the existing approaches; it is focused on the determination of an accurate path of the ego-vehicle, especially while maneuvering. The estimation of the path prediction is achieved through a hierarchical-structured fusion algorithm that allows the efficient use of the available sources of information and reduces the uncertainties introduced by the use of a single source. The available information sources include the status of the vehicle (vehicle dynamics) and the status of the road (road boundaries); they are both estimated by sensor measurements and multiple vehicle and road models, respectively.

The information fusion process is carried out in two levels, as shown in Fig. 1. At level 1, paths are estimated using a homogeneous information: A path is estimated based on vehicle dynamics and adaptive multiple models, while an alternative path is estimated based on the road geometry, taking into account the detection of stationary objects [hereafter called as road borders (RBs) model] and the trails of the moving vehicles [hereafter called as scene tracking (ST) model]. At level 2, the information fusion process is the combination of the estimated paths using *a priori* knowledge and online situation models.

In addition, an advantage of the approach is the fact that it introduces the time evolution of the kinematic attributes of the ego-vehicle. Should the same approach be applied for the estimation of the path of the frontal moving objects,[1] a dynamic threat assessment algorithm could be adopted. Consequently, the purpose of the approach is to enhance the capabilities of ACC and FCW systems and to extend the operational scenarios to cutting-in situations, up to a range of 150 m ahead [i.e., the range of a typical millimeter-wave (MMW) radar].

[1]It is not in the scope of this paper. It needs a special treatment due to the different measurement space and the limitations of the sensor system (e.g., the radar is incapable of estimating lateral dynamics, which causes additional uncertainties to the system).

The remainder of this paper is organized as follows. In Section II, the mathematical tools and the notation are described for level 1 of the fusion process, regarding the vehicle-dynamics-based path prediction. Emphasis is given on the development of new motion models of the ego-vehicle to provide a robust path when other source of information is missing. In Section III, details are given on how to use road models for the estimation of the vehicle's path, based on sensor input for the lateral displacement. In Section IV, the complete hierarchical approach is described, and results are given through normal test trials. In Section V, the EUCLIDE application (CW and vision enhancement) is presented, and conclusions are drawn.

In each chapter, results from real-world data and various traffic situations are given for the validation of the proposed algorithms. The dedicated data collection sessions were carried out in highways, extra urban, and rural roads. Two different platforms were used: The first one was a Fiat experimental vehicle, and the second one was a Volvo research car. Both are equipped with an infrared camera, high-resolution imaging radar, and inertial sensors. Due to the lack of ground truth data, a new method is proposed for the offline calculation of the true trajectory of the ego-vehicle, and it is presented in annex 1.

II. Path Prediction Based on Vehicle Dynamic Models

In the proposed approach, in order to introduce the evolution of the ego-path in time, the state of the ego-vehicle in the near future is defined in a state space. Let x be a state vector that describes the dynamic state of a vehicle. Its future state can be estimated using a motion model, as shown in the following equation:

$$x(k+1) = A(k) \cdot x(k) + w(k) \tag{1}$$

where $x(k+1)$ and $x(k)$ are the state vectors of the vehicle at scans $k+1$ and k, respectively, w is the Gaussian zero mean process noise with a covariance Q, and $A(k)$ is the transition matrix of the selected model that is computed at scan k. In the case of nonlinear models, where the update equation is given by the closed-form solution $x(k+1) = f[x(k)]$, the transition matrix can be computed through its Jacobian $A(k) = \partial f[x(k)]/\partial x(k)$.

The equation used for the propagation of the covariance error and the evaluation of the reliability of the estimated path is the following:

$$P(k+1) = A(k) \cdot P(k) \cdot A(k)^T + Q. \tag{2}$$

It is assumed that the estimated trajectory has a fixed number of points, which is equal to N_p. The time step T between two successive predicted scans is fixed and is usually set to 0.1 s, without any loss of generality. The algorithm is applied at every scan of the data sequence, performing a prediction for the next $N_p \cdot T$ seconds with respect to the current vehicle coordinate system. The coordinate system has its center located in the middle of the bumper of the ego-vehicle, while its x-axis is parallel to the longitudinal axis (ISO coordinate system).

A. Vehicle Filter

A Kalman filter is used to track the dynamic state of the vehicle at every scan. The state vector that is used in the filter consists of six state space variables and is the following:

$$x(k) = [U \quad A \quad \dot{A} \quad \varphi \quad \omega \quad \dot{\omega}]^T \tag{3}$$

where U is the vehicle's speed, A is its acceleration, $\dot{A}$ is the derivative of the acceleration, φ is the vehicle's yaw angle, ω is the yaw rate, and $\dot{\omega}$ is the yaw acceleration. The measurements that are provided by the inertial sensors to the CAN bus are the vehicle's speed and yaw rate. Thus, the measurement vector will be the following: $y = [U \quad \omega]^T$. The mapping from the measurement space to the state space is linear, and the measurement matrix is

$$C = \begin{bmatrix} 1 & 0 & 0 & 0 & 0 & 0 \\ 0 & 0 & 0 & 0 & 1 & 0 \end{bmatrix}. \tag{4}$$

The covariance matrix of the zero mean, white, and Gaussian measurement noise is

$$R = \begin{bmatrix} \sigma_U^2 & 0 \\ 0 & \sigma_\omega^2 \end{bmatrix} \tag{5}$$

where σ_U and σ_ω are the standard deviation for the measurement noise of the velocity and the yaw rate, respectively. The model chosen for the state equation update considers a constant acceleration (CA) derivative and a constant derivative of the yaw rate so that the transition matrix of the state equation is

$$A = \begin{bmatrix} 1 & T & 0.5 \cdot T^2 & 0 & 0 & 0 \\ 0 & 1 & T & 0 & 0 & 0 \\ 0 & 0 & 1 & 0 & 0 & 0 \\ 0 & 0 & 0 & 1 & T & 0.5 \cdot T^2 \\ 0 & 0 & 0 & 0 & 1 & T \\ 0 & 0 & 0 & 0 & 0 & 1 \end{bmatrix}. \tag{6}$$

The covariance matrix of the process noise will be $Q = G \cdot q \cdot G^T$, where the matrix G is

$$G = \begin{bmatrix} 0.5 \cdot T^2 & T & 1 & 0 & 0 & 0 \\ 0 & 0 & 0 & 0.5 \cdot T^2 & T & 1 \end{bmatrix}^T \tag{7}$$

and the matrix q is

$$q = \begin{bmatrix} \sigma_{\dot{A}}^2 & 0 \\ 0 & \sigma_{\dot{\omega}}^2 \end{bmatrix} \tag{8}$$

where we assumed a zero mean, white, and Gaussian process noise, with variances $\sigma_{\dot{A}}^2$ and $\sigma_{\dot{\omega}}^2$ for the derivative of the acceleration and the yaw acceleration, respectively. In cases where the velocity is changing with a high rate, the filter that has been described is not able to estimate the velocity, and thus, a different approach is needed. The solution that is proposed by Bar-Shalom *et al.* in [7, p. 424] is that the process noise switches between three predefined values, according to the input. Three thresholds are set and define the levels of the covariance elements that are used to calculate the respective covariance matrix. The respective level of process noise is assigned to the derivative of the acceleration, according to the current value of the acceleration, which is compared at every scan with the defined thresholds. The same technique cannot be applied in the case of the yaw rate because of the fact that its value is changing much more frequently compared to the velocity, and it causes biases to the filter.

B. Dynamic Models for the Ego-Motion

There are three models that are used in estimating the future path of a vehicle. Each one makes an assumption for one of the basic state space variables (acceleration and turn rate). The first one is the CA, the second one is the constant yaw rate, and finally, the last one, which may be considered as the generalization of the two previous models, assumes that both acceleration and turn rate remain constant over time. The latter belongs to the family of curvilinear models [8].

1) CA Model: The first dynamic model that is used for predicting the future trajectory of the vehicles is the CA model. In this model, the acceleration of the vehicle is assumed to be constant in both axes. The transition matrix A_{CA} for this model is

$$A_{\mathrm{CA}} = \begin{bmatrix} 1 & T & 0.5 \cdot T^2 & 0 & 0 & 0 \\ 0 & 1 & T & 0 & 0 & 0 \\ 0 & 0 & 1 & 0 & 0 & 0 \\ 0 & 0 & 0 & 1 & T & 0.5 \cdot T^2 \\ 0 & 0 & 0 & 0 & 1 & T \\ 0 & 0 & 0 & 0 & 0 & 1 \end{bmatrix}. \tag{9}$$

The state vector is formed using the position, velocity, and acceleration in both axes. Thus, the initial state vector that is used to predict the future path of the subject vehicle is

$$x(0) = [0 \quad U_V \quad A_V \quad 0 \quad 0 \quad \omega_V \cdot U_V]^T \tag{10}$$

where U_V, A_V, and ω_V are the current velocities, acceleration, and turn rate, respectively, that are estimated by the vehicle filter described in the previous section.

2) Constant Turn Rate (CTR) Model: In this case, it is assumed that the yaw rate and the speed of the vehicle remain constant over time. The main equation describing this model gives the rate of change of the acceleration vector $\dot{A}$ in terms of the turn rate ω and the velocity vector U as $\dot{A} = -\omega^2 \cdot U$. The yaw rate ω, which is used in the previous equation, is given by the following cross product $\omega = (U \times A)/|U|^2$. The two previous equations can describe the basic dynamic behavior of an object that is performing a coordinate turn [9]. In the following analysis, it is assumed that the acceleration is normal to the velocity vector, and the motion is in the x–y horizontal plane. The velocity of the vehicle can be analyzed in its components that are defined in terms of the velocity magnitude U and the heading angle φ:

$$U_X = U \cdot \cos(\varphi) \quad \text{and} \quad U_Y = U \cdot \sin(\varphi). \tag{11}$$

Considering the special case of acceleration that is normal to the velocity, the velocity will remain constant. Differentiating twice, it yields to the following set of equations:

$$A_x = \dot{U}_X = -U \cdot \omega \cdot \sin(\varphi) = -\omega \cdot U_Y \tag{12a}$$

$$\dot{A}_X = -U \cdot \omega^2 \cdot \cos(\varphi) = -\omega^2 \cdot U_X \tag{12b}$$

$$A_Y = \dot{U}_Y = U \cdot \omega \cdot \cos(\varphi) = \omega \cdot U_X \tag{12c}$$

$$\dot{A}_Y = -U \cdot \omega^2 \cdot \sin(\varphi) = -\omega^2 \cdot U_Y. \tag{12d}$$

The state prediction equations are derived, assuming a CTR $\omega = \dot{\varphi}$:

$$\begin{aligned} x(k+1) &= x(k) + \int_{t_k}^{t_{k+1}} U_X(\tau|t_k)d\tau \\ &= x(k) + T \cdot [\text{SW} \cdot U_X(k) - \text{CW} \cdot U_Y(k)] \end{aligned} \tag{13a}$$

$$\begin{aligned} y(k+1) &= y(k) + \int_{t_k}^{t_{k+1}} U_Y(\tau|t_k)d\tau \\ &= y(k) + T \cdot [\text{CW} \cdot U_X(k) + \text{SW} \cdot U_Y(k)] \end{aligned} \tag{13b}$$

where $\text{SW} = \sin(\omega \cdot T)/(\omega \cdot T)$, and $\text{CW} = [1 - \cos(\omega \cdot T)]/(\omega \cdot T)$. Similarly, for velocity

$$\begin{aligned} U_X(k+1) &= U \cdot \cos(\varphi + \omega \cdot T) \\ &= U_X(k) \cdot \cos(\omega \cdot T) \\ &\quad - U_Y(k) \cdot \sin(\omega \cdot T) \end{aligned} \tag{14a}$$

$$\begin{aligned} U_Y(k+1) &= U \cdot \sin(\varphi + \omega \cdot T) \\ &= U_X(k) \cdot \sin(\omega \cdot T) \\ &\quad + U_Y(k) \cdot \cos(\omega \cdot T). \end{aligned} \tag{14b}$$

Thus, the closed-form solution of the update equation for this model will have the following form:

$$\begin{bmatrix} x(k+1) \\ U_X(k+1) \\ y(k+1) \\ U_Y(k+1) \\ \omega(k+1) \end{bmatrix} = \begin{bmatrix} x(k) + T \cdot [\text{SW} \cdot U_X(k) - \text{CW} \cdot U_Y(k)] \\ U_X(k) \cdot \cos(\omega(k) \cdot T) - U_Y(k) \cdot \sin(\omega(k) \cdot T) \\ y(k) + T \cdot [\text{CW} \cdot U_X(k) + \text{SW} \cdot U_Y(k)] \\ U_X(k) \cdot \sin(\omega(k) \cdot T) + U_Y(k) \cdot \cos(\omega(k) \cdot T) \\ \omega(k) \end{bmatrix}. \tag{15}$$

The linearization method that is described at the beginning is applied, and the resulting transition matrix is given by the following:[2]

$$A = \begin{bmatrix} 1 & \sin(\omega T)/\omega & 0 & -(1-\cos(\omega T))/\omega & f_{15} \\ 0 & \cos(\omega T) & 0 & -\sin(\omega T) & f_{25} \\ 0 & (1-\cos(\omega T))/\omega & 1 & \sin(\omega T)/\omega & f_{35} \\ 0 & \sin(\omega T) & 0 & \cos(\omega T) & f_{45} \\ 0 & 0 & 0 & 0 & 1 \end{bmatrix}. \tag{16}$$

The state vector is formed using the position and the velocity of the vehicle in both axes and its turn rate. Thus, the initial state vector that is used in estimating the future trajectory of the subject vehicle is

$$x(0) = [0 \quad U_V \quad 0 \quad 0 \quad \omega_V]^T. \tag{17}$$

The same vector, when the model is applied in a tracked object to find its future path, will have the following form:

$$x(0) = \left[x_0 \quad U_X \quad y_0 \quad U_Y \quad \frac{U_X \cdot A_Y - U_Y \cdot A_X}{U_X^2 + U_Y^2}\right]^T \tag{18}$$

where $[x_0 \ U_X \ A_X \ y_0 \ U_y \ A_y]^T$ is the estimated state vector of the tracked object (position, velocity, and acceleration in both axes).

3) Constant Turn Rate Constant Tangential Acceleration Model (CTRA): The third dynamic model that is used is the CTRA model. This model describes, with a more realistic manner, the true motion of a vehicle as it considers that it is moving with a constant tangential acceleration A_T and constant yaw rate ω. It is assumed that the speed is changing with a constant rate, which is the tangential acceleration, while the object's turn rate also remains constant over time $A_T = \dot{U}$ and $\omega = \dot{\varphi}$. The two overall-acceleration components are computed as follows:

$$\begin{aligned} A_X &= \dot{U}_X \\ &= \dot{U} \cdot \cos(\varphi) - U \cdot \dot{\varphi} \cdot \sin(\varphi) \\ &= A_T \cdot \cos(\varphi) - \omega \cdot U \cdot \sin(\varphi) \\ &= A_T \cdot \cos(\varphi) - \omega \cdot U_Y \\ &= A_{TX} + A_{CX} \end{aligned} \tag{19a}$$

[2]

$$d\text{sw} = \frac{\cos(\omega T)}{\omega} - \frac{\sin(\omega T)}{\omega^2 T} \tag{16a}$$

$$d\text{cw} = \frac{\sin(\omega T)}{\omega} - \frac{1}{\omega^2 T} + \frac{\cos(\omega T)}{\omega^2 T} \tag{16b}$$

$$f_{15} = \frac{\partial x}{\partial \omega} = T \cdot (U_x \cdot d\text{sw} - U_y \cdot d\text{cw}) \tag{16c}$$

$$f_{25} = \frac{\partial U_x}{\partial \omega} = -T \cdot (U_x \cdot \sin(\omega T) + U_y \cdot \cos(\omega T)) \tag{16d}$$

$$f_{35} = \frac{\partial y}{\partial \omega} = T \cdot (U_x \cdot d\text{cw} + U_y \cdot d\text{sw}) \tag{16e}$$

$$f_{45} = \frac{\partial U_y}{\partial \omega} = T \cdot (U_x \cdot \cos(\omega T) - U_y \cdot \sin(\omega T)) \tag{16f}$$

$$\begin{aligned} A_Y &= \dot{U}_Y \\ &= \dot{U} \cdot \sin(\varphi) + U \cdot \dot{\varphi} \cdot \cos(\varphi) \\ &= A_T \cdot \sin(\varphi) + \omega \cdot U \cdot \cos(\varphi) \\ &= A_T \cdot \sin(\varphi) + \omega \cdot U_X \\ &= A_{TY} + A_{CY}. \end{aligned} \tag{19b}$$

Therefore, the two centripetal acceleration components (normal to the vehicle's motion) will be given from the following relationships: $A_{CX} = -\omega \cdot U_Y$ and $A_{CY} = \omega \cdot U_X$. Apparently, it is easily seen that

$$\begin{aligned} A_C &= \sqrt{A_{CX}^2 + A_{CY}^2} \\ &= \sqrt{\omega^2 \cdot U_Y^2 + \omega^2 \cdot U_X^2} \\ &= \omega \cdot \sqrt{U_X^2 + U_Y^2} \\ &= \omega \cdot U. \end{aligned} \tag{20}$$

In turn, the two components of the tangential acceleration are computed as $A_{TX} = A_T \cdot \cos(\varphi)$ and $A_{TY} = A_T \cdot \sin(\varphi)$. Using the aforementioned assumptions and the basic equations of the model, a closed-form solution of the state update equation is extracted, and by applying the linearization method, it is found that the transition matrix of the model is equal to (21), shown at the bottom of the page. The definition of $f(ij)$ parameters is given in [12]. The state vector of this model is formed using the position, velocity and acceleration in both axes, and the turn rate of the vehicle. Thus, initially, the state vector in the case of the subject vehicle will be

$$x(0) = [0 \quad U_V \quad A_V \quad 0 \quad 0 \quad 0 \quad \omega_V]^T. \tag{22}$$

4) Adaptive Dynamic (AD) Model: It is expected that the CA model will succeed in predicting the future path in the cases where the driver is moving with a constant longitudinal acceleration. In turn, the CTR model will succeed when the driver is making a turn with a CTR, while the CTRA model will predict the future path correctly when the driver is turning with a constant yaw rate while he is accelerating. Heuristic rules are proposed and implemented by examining the data from real driving recordings, which give the opportunity for the right model to be applied to the right scenario. The model that is applied to estimate the future path is adapted to the derivative of the yaw rate and the longitudinal acceleration (optimizing the performance of the model in the lateral and longitudinal axes, respectively). The selected values for the model switching process are 0.01 rad/s^2 and 0.05 m/s^2. For example, if $(\partial\omega/\partial t) > 0.01$ rad/s^2 and $A_X > 0.05$ m/s^2, the CTRA model is assigned; otherwise, if $(\partial\omega/\partial t) < 0.01$ rad/s^2, the CA model is applied; otherwise, the CTR model is applied.

This adaptive model, based on the three dynamic submodels, has the smallest root mean square error (rms), comparing its performance with the three models. It should be noted that, for ACC systems, only the rms error in the x-axis should be considered, as the field of view of the radar that is used in such systems is very narrow, but for the general collision avoidance case, rms errors in both axes should be taken into account.

III. Path Prediction Based on Road Boundaries Models

A. Models for Road Boundaries

The data that is used to derive the model for the road boundaries consists of the detected stationary objects from a radar. The most common model that mathematically describes the geometrical structure of the RBs is the clothoid model. Clothoid is used to define a curve; its curvature c is a linear function of the curve's arc length l: $c(l) = c_0 + c_1 \cdot l$, where c_0 is the initial curvature, and c_1 is the curvature's rate. The clothoid can also be defined using the following expressions:

$$x(l) = \int_0^l \cos\left(c_o\tau + \frac{c_1\tau^2}{2}\right) d\tau \tag{23a}$$

$$y(l) = y_0 + \int_0^l \sin\left(c_o\tau + \frac{c_1\tau^2}{2}\right) d\tau. \tag{23b}$$

A clothoid can be approximated by a third-order polynomial, which is as follows:

$$y(x) = c_0\frac{x^2}{2} + c_1\frac{x^3}{6} + y_0 \tag{24}$$

where y_0 is the offset from the subject vehicle's position. It is obvious that, for the proper modeling of the RBs, two different offsets must be computed, i.e., one for the left y_{0L} and one for the right border y_{0R}. With regard to the curvature and the

$$A_{\mathrm{CTRA}} = \begin{bmatrix} 1 & \frac{\sin(\omega T)}{\omega} & f(13) & 0 & \frac{\cos(\omega T)-1}{\omega} & f(16) & f(17) \\ 0 & \cos(\omega T) & T\cos(\omega T) & 0 & -\sin(\omega T) & -T\sin(\omega T) & f(27) \\ 0 & 0 & \cos(\omega T) & 0 & 0 & -\sin(\omega T) & f(37) \\ 0 & \frac{1-\cos(\omega T)}{\omega} & f(43) & 1 & \frac{\sin(\omega T)}{\omega} & f(46) & f(47) \\ 0 & \sin(\omega T) & T\sin(\omega T) & 0 & \cos(\omega T) & T\cos(\omega T) & f(57) \\ 0 & 0 & \sin(\omega T) & 0 & 0 & \cos(\omega T) & f(67) \\ 0 & 0 & 0 & 0 & 0 & 0 & 1 \end{bmatrix} \tag{21}$$

curvature's rate, their values will be the same for both borders. Thus, the state vector that is used to describe the road is

$$x_{\mathrm{RB}} = [c_0 \quad c_1 \quad y_{0L} \quad y_{0R}]^T. \tag{25}$$

The state update equation is formed using the current coordinate system; thus, it is necessary to take into account the displacement of the subject vehicle using its estimated state and considering that the vehicle's motion is done on the basis of the CA model. The high-resolution radar that is used, being able to receive echoes from RBs (e.g., posts, grass, guardrails, etc.), has the capability of "imaging"; the detections suffer from a high clutter which affects the assignment of the measurements to the RBs estimator. In the literature, such algorithms have been proposed for laser scanners or imaging systems (i.e., CMOS/CCD cameras) and very few for radars [3].

B. Estimation of the Lateral Offset and Road Width

The detections coming from the radar are not smooth at all; the result is that the estimation of the clothoid filter is not applicable in other processing tasks, or in some cases, there is no estimation at all. A second filter is used, which considers the output of the clothoid filter as measurements, and its role is to provide smoothed values for the lateral offset from the road sides and to estimate the lateral velocity. The state vector that is used in this Kalman filter is formed from five state variables and is as follows:

$$x_{\mathrm{RF}} = [d_L \quad u_L \quad d_R \quad u_R \quad w]^T \tag{26}$$

where d_L is the distance from the left road side, u_L is the left lateral speed of the vehicle, d_R is the distance from the right side of the road, u_R is the right lateral speed, and w is the width of the road. It must be noted that the left and right lateral speeds are the derivatives of the left and right distances, respectively. The dynamic model that is proposed for the state equation update leads to an uncorrelated estimation between the road width and the two lateral offsets. The process noise covariance matrix is

$$Q = G \cdot q \cdot G^T \tag{27}$$

where the matrix G will be given from $G = \begin{bmatrix} T & 1 & 0 & 0 & 0 \\ 0 & 0 & T & 1 & 0 \\ 0 & 0 & 0 & 0 & 1 \end{bmatrix}^T$, and the matrix q will be computed as $q = \mathrm{diag}(\sigma_{UL}^2, \sigma_{UR}^2, \sigma_W^2)$, where σ_{UL}^2 is the variance of the left lateral speed process noise, σ_{UR}^2 is the variance of the right lateral speed process noise, and σ_W^2 is the variance of the road width process noise. During the estimation of the width, a very low process noise is applied because the real road width is practically constant. The measurement vector of the filter consists of the left d_{Lm} and right d_{Rm} lateral offsets that are provided by the clothoid filter: $y = [d_{Lm} \quad d_{Rm}]^T$. The measurement matrix that is used to map the measurement space to the state space is $C = \begin{bmatrix} 1 & 0 & 0 & 0 & -1 \\ 0 & 0 & 1 & 0 & 1 \end{bmatrix}^T$, where the left offset is considered to have negative values, and the right offset is considered to have positive values. The two measurement variables are considered to be received from the first filter (clothoid) with uncorrelated Gaussian zero mean error and variances σ_{Lm}^2 and σ_{Rm}^2, respectively. Thus, the measurement covariance matrix is $R = \mathrm{diag}(\sigma_{Lm}^2, \sigma_{Rm}^2)$.

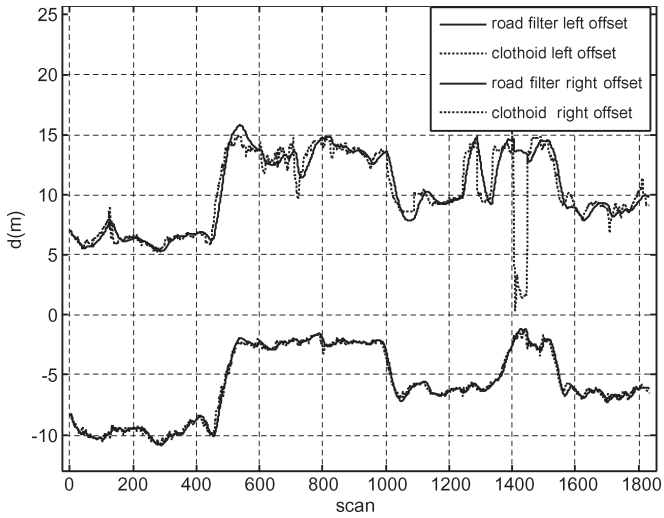

Fig. 2. Output of the road filter in a highway scenario.

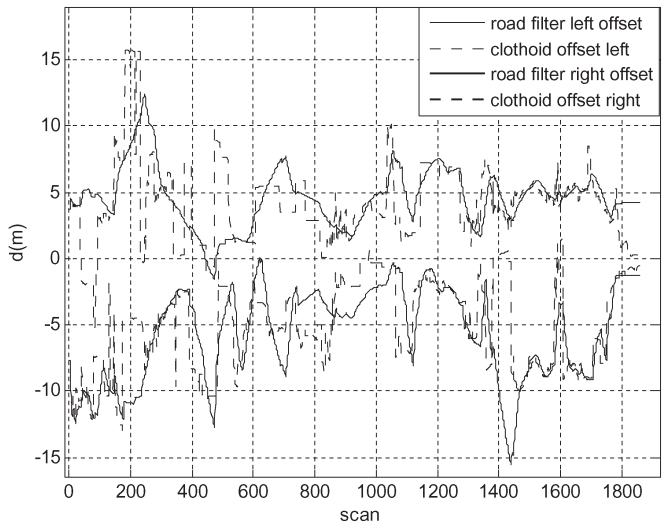

Fig. 3. Output of the road filter in a rural scenario.

In case the clothoid filter fails to give an estimation of the lateral offsets, then the estimated values from the previous scan are used. Finally, there are two levels of process noise. The first one is used when the filter runs in normal conditions, and the second one—which is much lower—is used when one side of the road is not detected. Results from the road filter are shown in Figs. 2 and 3 for a highway and rural road scenario. The use of the secondary filter in cases where the subject vehicle is moving in extra urban or rural roads may significantly improve the estimation of the road geometry and avert fault estimates or even complete estimate failures.

In Section IV, this filter will be used in deriving a situation model for lateral maneuvers of the drivers.

C. RB and Combinational Dynamics and RB (CDRB) Path Prediction Models

Should we assume that the vehicle is following the road geometry, then the future path of the vehicle can also be computed by taking into account the detected geometry of the RBs or the lanes detected by a vision system. In the longitudinal axis, the update of the dynamic state of the vehicle is done using a dynamic model, which is usually the CA model due to its good performance and the low computational cost, while in the lateral axis, the motion of the vehicle is described using the equation of the road, i.e., clothoid model described in Section III-B. The equations that are used to estimate the trajectory are the following:

$$y = y_0 + \frac{1}{2}\cdot c_0 \cdot x^2 + \frac{1}{6}\cdot c_1 \cdot x^3 \tag{28a}$$

$$x = x_0 + U_0 \cdot t + \frac{1}{2}\cdot A \cdot t^2. \tag{28b}$$

The state update equations will have the following form:

$$A_X(k+1) = A_X(k) \tag{29a}$$

$$U_X(k+1) = U_X(k) + A_X(k)\cdot T \tag{29b}$$

$$x(k+1) = x(k) + U_X(k)\cdot T + 0.5\cdot A_X(k)\cdot T^2 \tag{29c}$$

$$y(k+1) = y(k) + \frac{1}{2}\cdot c_0 \cdot x^2(k+1) + \frac{1}{6}\cdot c_1 \cdot x^3(k+1) \tag{29d}$$

where c_0 and c_1 are the estimated curvature and curvature rate, respectively, using the clothoid algorithm that is applied to the radar or camera detections. The state vector is formulated using the velocity and acceleration in the x-axis and the position of the vehicle in both axes. The initial state vector will be given from $\underline{x} = [x_0 \quad U \quad A \quad y_0]^T$. The ideal scenarios, where this model will predict the future path with a very small rms error, are those in which the driver is following the road geometry, that is to say, when he/she is not performing maneuvers such as lane changes, drifting, or overtaking. The model that is described using (29) will be, hereafter, refer to as the RB model for path prediction.

This paper introduces a new model that is applied in the y lateral axis and combines, in a weighted manner, the road-following behavior of a driver and the possibility of maneuvering. The so-called CDRB model makes use of a weight to sum up the displacements of the two different models in order to predict the future path. The weight that is used to correlate vehicle dynamics and RBs is defined as

$$r = \frac{N_p - k}{N_p - 1}, \qquad k = 1, 2, \ldots, N_p \tag{30}$$

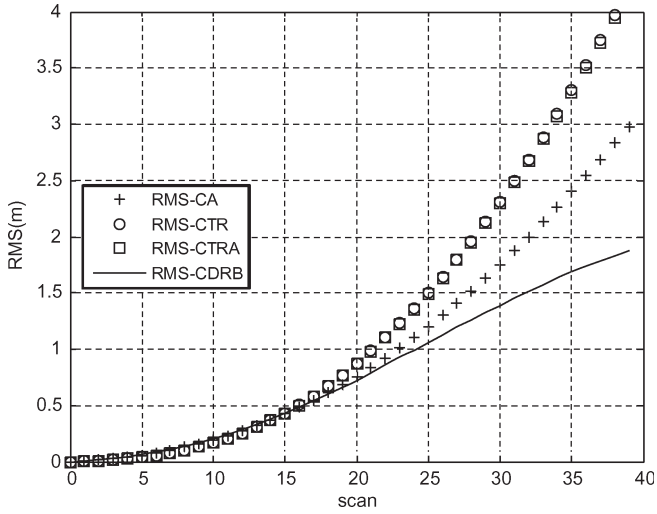

Fig. 4. RMS trajectory error for dynamic and CDRB models at the end of an overtake maneuver.

where N_p are the future time instances/points of the path. The predicted trajectory is then calculated using the following relationships:

$$x(k) = x_d(k) \tag{31a}$$

$$y(k) = r\cdot y_d(k) + (1-r)\cdot y_r(k), \qquad k = 1, 2, \ldots, N_p \tag{31b}$$

where x_d is the position that is calculated using the dynamic model, y_r is the position that is calculated using the RBs model, and y_d is the lateral displacement that is calculated by the dynamic model. This model, as will be shown later, is suitable for cases when the driver performs a maneuver since it gives more weight—in a linear sense [cf., (30)]—to the actual vehicle dynamics at the beginning of the maneuver.

The advantages of the CDRB model are more obvious in cases such as the beginning and the end of road segments with high curvatures or the overtaking maneuvers of other vehicles—specifically at the beginning and at the end of the overtaking maneuver—and in lane changes with small lateral speed values. The combinational model can be compared with the other three dynamic models using the rms trajectory of the predicted path of the subject vehicle. In Figs. 4 and 5, an overtaking maneuver is presented. The maneuver can be separated in three phases. The first phase is the lane change to the left, the second phase is the motion that is parallel to the borders to overtake the leading vehicle, and the third one is the lane change to the right. By examining the figures of the third phase of the maneuver, it can be seen that the CDRB model has a smaller rms error from the dynamic models. The same results are extracted for the first phase, as it is the same type of movement but in the opposite direction. In the second phase, dynamic or RB models are also adequate.

The advantages of the CDRB reveal that it should be applied when the yaw rate is changing rapidly to a higher or lower level; such a situation may occur when the vehicle is entering or exiting a curve which has a high curvature or when the subject vehicle is changing lanes. The combinational path must

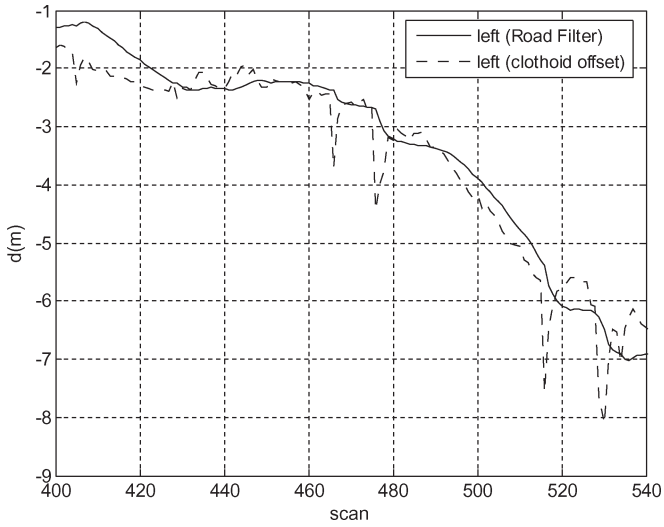

Fig. 5. Estimated left offset during a lane change.

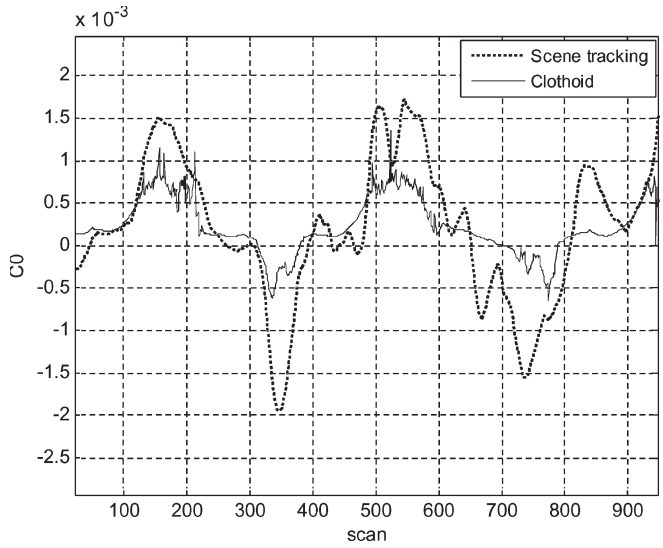

Fig. 6. Comparative study of the scene tracker and the clothoid filter in a highway scenario.

be the choice for the estimation of the future path when an overtaking maneuver is detected and, specifically, at the start and end points of the overtaking maneuver. On the other hand, when the vehicle is moving straight, the dynamic model has an increased accuracy due to the simplicity of the motion, which is greater than the road estimation accuracy, and there is no need to use the combined model.

To conclude this section, one should admit that there should be a way to identify the situation of the ego-vehicle so that the correct model is assigned at any time. This problem is addressed in Section IV, where the information fusion process is described.

In Section III-D, an additional approach is presented, which belongs to the same group of RBs models.

D. ST Model

The main assumption of this algorithm is the fact that traffic flow is following the road boundaries. An increased performance is achieved if there is a large number of leading vehicles and if the leading vehicles are not performing maneuvers. The representation of the traffic flow can be modeled by creating a buffer for each leading vehicle and by saving in the buffers the position estimates of all vehicles in every scan. All the buffers must be updated in every scan using the subject vehicle's velocity, heading, yaw rate, and acceleration since the coordinate system is relative to the current orientation of the subject vehicle, and the coordinate system is changing over time.

Let N_{TO} be the number of all the tracked objects that are moving inside the RBs and are moving in the same direction as the subject vehicle. For each one, a buffer B_i $(i = 1, 2, \ldots, N_{\mathrm{TO}})$ is formulated using the position estimations. The buffer can be considered as a stack where the most recent estimation is inserted at the top. If it is assumed that a fixed length N_B for the buffer must be retained, then if the number of the total elements that are included in the stack exceeds the limit, the last one is deleted. In each scan, before the insertion of the new position element $(x, y)_i$ in the stack, the old position values $(x_j, y_j)_i$ $(j = 1, 2, \ldots, N_B)$ must be updated using the vehicle's displacement as follows: $dx = 0.5 \cdot \omega \cdot V \cdot T^2$ and $dy = V \cdot T + 0.5 \cdot A \cdot T^2$, where $[V \quad A \quad \omega]^T$ is the vehicle's state (velocity, acceleration, and yaw rate). The CA model was used to update the position of the subject vehicle. In turn, the transition to the new coordinate system is done as follows—taking into consideration the $d\varphi$ (rad) change in the heading of the subject vehicle:

$$x_{ji}(k+1) = \lfloor x_{ji}(k) - dx \rfloor \cdot \cos(d\varphi) - \lfloor y_{ji}(k) - dy \rfloor \cdot \sin(d\varphi) \tag{32a}$$

$$y_{ji}(k+1) = [y_{ji}(k) - dy] \cdot \cos(d\varphi) + [x_{ji}(k) - dx] \cdot \sin(d\varphi). \tag{32b}$$

Once the position update is achieved, the insertion of the new position estimate in the buffer follows. Then, the algorithms make some checks, i.e., the number of the tracked objects and the length of the buffer, by finding the distance between the first and last position elements in the stack. If this distance is greater than a fixed threshold, then the buffer is valid for further processing. All the buffers that are being marked as "valid" are merged into one global buffer after being transformed to the current coordinate system, according to (32). The global buffer contains the past trails of all the tracked objects. The elements of the global buffer are sorted according to the x coordinate of all the position elements, and finally, a Kalman estimator is applied by using the buffer as the measurement space of the clothoid model estimator.

In Fig. 6, the benefits of the ST algorithm are shown in more detail. The scenario that is presented was recorded on a highway road. By comparing the two curvatures that are estimated using the ST algorithm and the clothoid filter, it is shown that the clothoid filter curvature can be enhanced using an ST curvature, in normal traffic conditions (objects not performing maneuvers), without a significant loss of information about the road

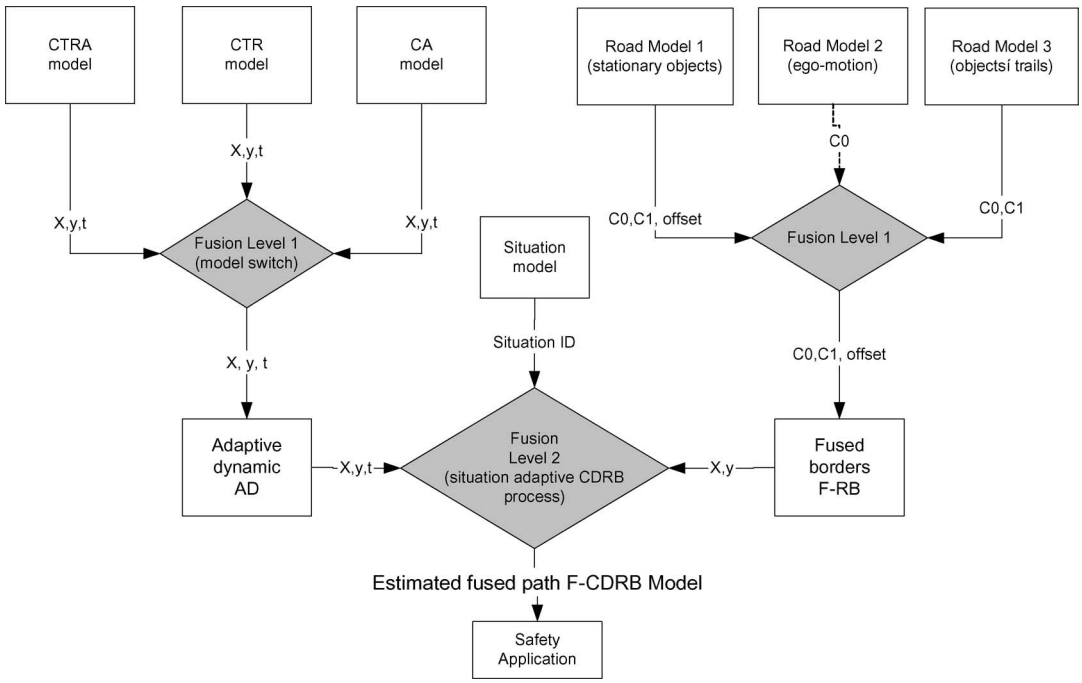

Fig. 7. Information fusion for the calculation of the path.

geometry. This is very useful for the cases where no estimated borders exist, such as when the vehicle is moving on rural roads.

The ST-based estimation of the future path of the subject vehicle (RB and CDRB models for path prediction) follows (28)–(31). x parameters are given from the dynamic model, and y parameters are given either from ST or the combinational rule of (30).

IV. Information Fusion System

The last step of the information fusion process is actually an extension of the CDRB model. The difference is that, instead of using only one dynamic model, it uses the AD model and that, instead of the RBs, it uses the fused data coming from the combination of the clothoid road geometry and the estimated geometry from the ST process, as described in Section III (hereafter named as F-RB). Its advantage is that, in cases that the estimation of RBs is biased or the measurement space is empty, the algorithm still does not fail as it is using the estimated curvature and curvature rate that are provided by the ST by assuming that at least one leading vehicle exists and that it is not maneuvering. Therefore, the efficient operation of the system to provide an accurate and reliable path of the subject vehicle is ensured, even when one of the sources of the road geometry is not providing estimations.

The general architecture of the system is shown in Fig. 7. The first level of the fusion process produces the AD model (Section II). The same is applied in the first fusion level of the road boundaries, which is estimated using either the RBs tracker (Section III-A) or the Kalman scene tracker (Section III-D). It must be noted that the curvature and curvature rate that are estimated from the scene tracker are taken into consideration for the prediction of the future path only until the last tracked object, whose buffer is included in the general buffer. The fusion between the two trackers is done using weights that are calculated by taking into account a normalized confidence measure of the two different methods. The yaw rate and the speed can be used to extract the curvature as an alternative method when the two previous methods fail to predict the road geometry.

In order to apply the second fusion step, a situation model is needed to assign the right model at any time, which produced the overall minimum error in the least square sense.

A. Situation Model

The situation model aims to detect maneuvers that lead to lane changes, excluding drifting or small lateral displacements. Here, the situation model is based on the filter of Section III-B, which estimates the lateral kinematics of the subject vehicle. As it will be shown, this model produces a robust diagnosis of lane changes. In the future, reasoning schemes could be proposed for the situation model for an enhanced performance.

More specifically, the method that is used to detect such maneuvers is based on the current estimation of the lateral speed. The estimation error of the left borders is greater than the error of the right ones due to the fact that the vehicle is moving to the right lane, and so, more guard rails will be detected on the right side of the road (greater accuracy of the estimated geometry); thus, the left lateral velocity from the filter is used. If the value of the lateral velocity gets over a predefined threshold U_M, then it can be assumed that the vehicle is starting to move toward the lateral axis.

$$\begin{aligned} &\text{If } u_L > U_M, && \text{then maneuver\_type} = \text{left} \\ &\text{if } u_L < -U_M, && \text{then maneuver\_type} = \text{right} \\ &\text{if } -U_M < u_L < U_M, && \text{then maneuver\_type} = \text{none.} \end{aligned} \tag{33}$$

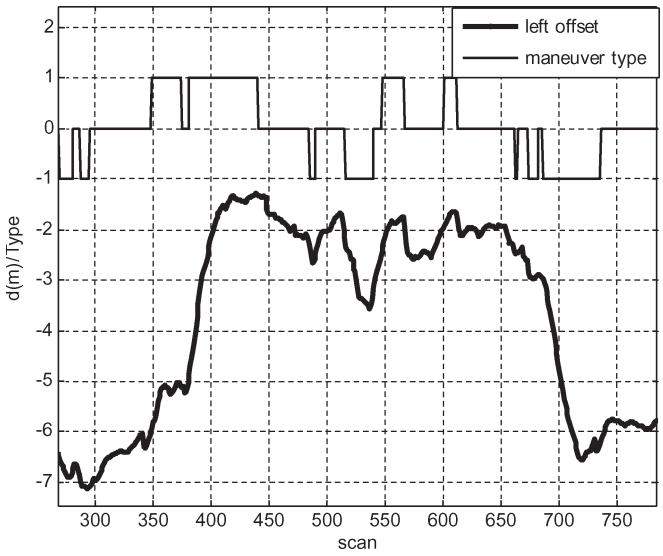

Fig. 8. Output of the maneuver detector.

A very small portion of the lateral velocity is caused by noise that exists in the lateral offset; therefore, the U_M threshold must properly be selected to avoid false detections in the case of existence of high levels of noise. Finally, the method that is proposed makes use of the lane width and the distance from the left side of the road to be able to detect lane changes. By dividing these two values, the lane of the subject vehicle can be found: LI $= [d_L/\text{LW}]$, where LI is the lane index, d_L is the distance from the left side of the road, LW is the lane width, and $[x]$ is the largest integer that is less than or equal to x (floor of x). Lane width is set to a constant value, is estimated by lane detection systems that the vehicle has, or is provided by the positioning system.

The performance of the situation model—maneuver detection algorithm—is shown in detail in Fig. 8, which includes an overtaking maneuver during the scans 350–750, where the distance from the left border and the output of the algorithm are shown. The specific overtaking includes an initial left lane change (there is a time period when the lane change is stopped momentarily), a straight line motion (interrupted by minor lateral displacements), and a right lane change in order to come back to the original lane. The entire three submaneuvers are efficiently detected, as shown in Fig. 8. In addition, the maneuver detection algorithm performance depends on the RBs estimation quality, and as a result, there might be some failures when the estimation error increases temporarily.

A separate trial is set up to define the threshold U_M that efficiently deals with the tradeoff of misses and false alarms. The trial is based on normal driving—cf., next paragraph for more details—data and video recording. Let, in our case study, a maneuver be defined when the overall lateral displacement $D_L > 0.5$ m for a time window of 10 s; the respective threshold for complete lane changes is defined as $D_L > 3$ m. Then, three values of U_M are selected for the trials 0.1, 0.25, and 0.5 m/s, and the situation model is applied. The performance measures are false alarms and system misses.

In Table I, the results of the trial are presented. A high value of U_M would eliminate the false alarms, but it fails to detect smaller maneuvers, not to mention that it fails to detect a significant number of lane changes (miss rate of 25%). On the other hand, a small threshold would create a number of false alarms; therefore, the 0.25 m/s value is selected.

TABLE I
RESULTS OF THE TRIALS FOR THE SELECTION OF THE THRESHOLD U_M

U_M	False alarms	Misses (maneuvers D_L >0.5m)	Misses (maneuvers D_L >3m)
0.1m/s	20%	5%	0%
0.25m/s	11%	20%	0%
0.5m/s	0%	98%	25%

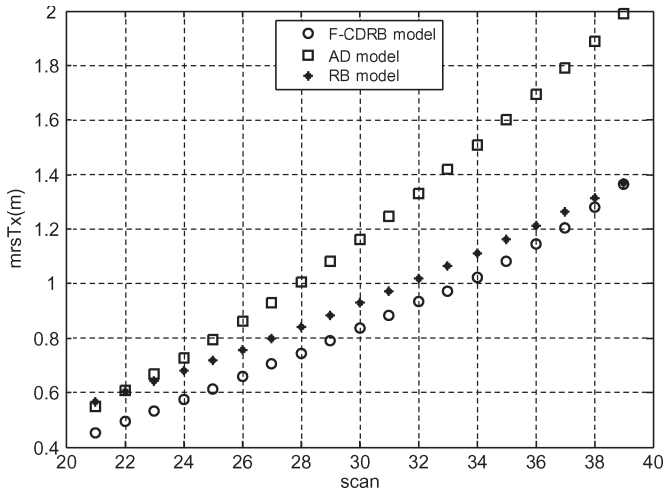

Fig. 9. RMS trajectory error comparison between the F-CDRB, AD, and RB models.

B. Performance of the System

The fused CDRB model (combining the AD model and the fused road boundaries F-CDRB) is, in turn, applied, given the fact that a maneuver is detected from the algorithm presented earlier. If this is not the case, then the fused RB (F-RB) model, or the AD in the absence of guardrails and tracked objects, is applied.

As an example, a 3-min recorded scenario (1800 system scans) is presented. During the scenario, the subject vehicle is following the road; in addition, it is performing several lane change maneuvers. In Fig. 9, the rms trajectory error is plotted for a fixed number of future path points (40—i.e., 4 s), and the results are shown for the F-RB, AD, and F-CDRB models. The use of the proposed information fusion architecture has resulted to the smallest rms error in an overall performance, although the maneuvering time is less than 10% of the duration of the complete scenario. This improvement is clearly shown if a time instant of a maneuver is examined. Such a time instant is shown in Fig. 10. It is shown that this approach predicts the maneuver before it actually happens, applies the fused model F-CDRB, and predicts that the subject vehicle will follow the road when the maneuver finishes. In the right figure, the respective AD-model-based estimated path is plotted for comparative reasons.

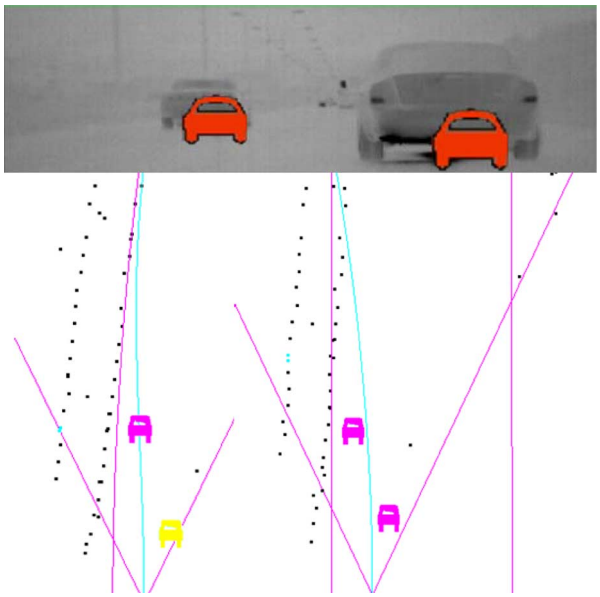

Fig. 10. Calculation of the estimated path in the time instant of an overtake maneuver using F-CDRB and dynamic models.

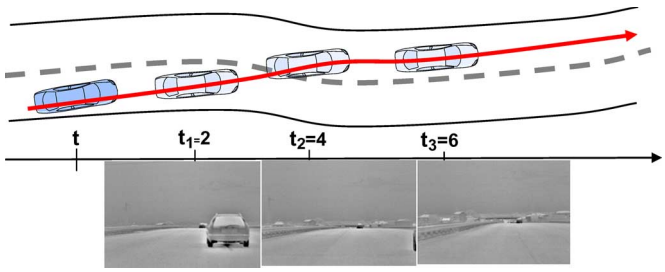

Fig. 11. Description of the test scenario for the evaluation of the information fusion process during lateral maneuvers.

It was shown that the overall performance of F-CDRB is superior to the individual path prediction models (10% less rms error). In addition, the performance of the system during lateral maneuver, i.e., where existing approaches fail, is worth investigating. In particular, 50 different naturalistic lane changes were recorded and examined through log files and video sequences. The recorded scenarios represent all types of lane changes, e.g., very slow, abrupt changes, overtaking maneuvers, etc.

The performance measure is the lateral offset $d_L(t)|_{t>t_0}$ of the estimated path with respect to the road boundaries. Let t_0 be the reference time that the path is estimated, which corresponds to a time instant where the maneuver is initiated by the driver. For each recorded lateral maneuver, three offsets are calculated $d_L(t_1)$, $d_L(t_2)$, and $d_L(t_3)$ at time instants $t_1 = 2$ s, $t_2 = 4$ s, and $t_3 = 6$ s, respectively, for CA, RB, and F-CDRB models. The values of t_1, t_2, and t_3 were selected to correspond to time instances during and after the lateral maneuver. Such time instances are shown in Fig. 11.

In this paper, and given the reference time, the lane changes are classified as "slow" when the duration of the maneuver $T_{\text{maneuver}} > 5$ s and as "fast," otherwise. The results of the experiment are shown in Tables II and III. In Table II, an example is given for slow and fast lane changes, while in Table III, statistics are given—average errors and standard deviation—for the total number of examined lane changes. F-CDRB detects the maneuver when the vehicle's lateral position is displaced by 20% in average of the overall displacement and assigns the correct model according to the proposed fusion hierarchies. The error of F-CDRB is 50–60 cm, which is independent of the future time instant, whereas RB and CA models have a significant error that varies a lot at time instances t_1, t_2, and t_3. The latter is obvious since each model addresses different phases of a lane change; the CA model behaves in a correct way during the lane changes (t_1 and t_2) and fails afterward (t_3), and the RB model behaves the other way around. One should note that, even then, F-CDRB is significantly superior due to the fact that it includes the first level of the fusion process (AD models and road boundaries fusion instead of CA and RB, respectively). The maximum of the error never exceeds 1 m, even in abrupt lane changes, which makes the algorithm suitable for vehicle to lane assignment.

V. Application Development

The work presented in this paper and the validation of the algorithm are based on large data sets that are acquired from two test vehicles from Volvo Cars and Fiat Research Centre, respectively, under the European cofunded research project EUCLIDE. The so-called EUCLIDE system has a vision enhancement and a forward CW function, merging the functionality of a far infrared camera and a high-resolution MMW radar sensor in order to warn the driver in case of lack of obstacle perception in adverse weather conditions. The driver in the EUCLIDE equipped cars perceives the danger through audible and visual signals (loudspeakers and a head-up-display). An example of the human–machine interaction is shown in Fig. 10, where the infrared image is displayed to the driver; in an additional layer, most dangerous objects are shown according to a dynamic threat assessment scheme [10]. The same figure, in the lower part, shows the future trajectory of the ego-vehicle during an overtake scenario using a simple dynamic model in the first case and the fused path F-CDRB in the second case.

The threat assessment in EUCLIDE functions was possible due to the dynamic calculation of path prediction that is presented in this paper and to a modified version of it for the moving objects. In EUCLIDE, objects are classified and assessed using two newly introduced parameters, which are directly derived from the prediction of paths, namely predicted minimum distance (PMD) and predicted time to minimum distance (TPMD); their definition is as follows.

1) PMD parameter is the minimum distance between a vehicle and a potential obstacle that is predicted in real time, e.g., if PMD=0, then an impact is forecasted.
2) TPMD parameter allows the classification of the level of danger and the assignment of different operating modes to the application.

The validation of the algorithms in this paper is based on the raw measurement data files and on processed data—signal/image processing and data fusion—for the extraction of the road characteristics and the state of the moving and stationary objects ahead. The algorithm for the extraction of the road

TABLE II
COMPARISON OF CA, RB, AND F-CDRB MODELS IN TWO LANE-CHANGE MANEUVERS

Maneuver Type	Future time instant (in sec w.r.t. the current position)	Actual Duration of the maneuver (s)	Error		
			Dynamic model (CA model)	Road boundaries model (RB model)	Fused path (F-CDRB model)
Lane Change maneuver 1	2	4	0.324	0.704	0.053
	4		0.948	0.863	0.427
	6		5.567	1.047	0.777
Overtaking maneuver 1	2	6	0.430	1.192	0.154
	4		0.330	2.170	0.075
	6		1.728	2.414	0.791

TABLE III
COMPARISON OF CA, RB, AND F-CDRB MODELS BASED ON 50 NATURALISTIC LANE CHANGES

Type	Future time instant (in sec w.r.t. the current position)	Calculation	Error		
			Dynamic model (CA model)	Road boundaries model (RB model)	Fused path (F-CDRB model)
50 naturalistic maneuvers	2	Average	0.624	1.372	0.495
	4		1.459	2.398	0.617
	6		4.957	2.436	0.636
	2	Standard deviation	0.517	0.555	0.416
	4		0.975	1.040	0.447
	6		2.605	0.771	0.582
"Slow maneuvers"	2	Average	0.377	1.027	0.228
	4		1.446	2.127	0.455
	6		3.353	2.823	0.559
	2	Standard deviation	0.143	0.291	0.151
	4		1.312	0.734	0.596
	6		1.107	0.766	0.498
"Fast maneuvers"	2	Average	0.788	1.602	0.672
	4		1.467	2.578	0.726
	6		6.026	2.179	0.687
	2	Standard deviation	0.622	0.587	0.450
	4		0.824	1.236	0.334
	6		2.838	0.720	0.674

geometry is briefly presented in this paper and in more details in [3]. A multisensor/multitarget tracking system is proposed for the object tracking [11], where several Kalman filters are working in parallel in a filter bank. For driving support application, the multisensor/multitarget tracking system is designed with the functionalities of data alignment, prediction, data association, measurement-to-track fusion, track initialization, track-to-track fusion, and elimination of tracks.

The situation-adaptive and dynamic calculation of the path prediction allowed the EUCLIDE system to extend and improve the functionalities of a conventional CW system in terms of the following: 1) correct assignment of the in-path object, especially while maneuvering; 2) minimizing the delay of warnings in cut-in situations; and 3) minimizing false alarms while maneuvering.

VI. CONCLUSION

This paper presents, in detail, a novel method that is used to calculate the path of the ego-vehicle in a dynamic situation adaptive way. The output space of the estimated path is 3-D (x, y, and t); it was shown that it is possible to predict the intention of the driver and estimate the path for the future 3–4 s with an accuracy less than 50 cm—always assigning the correct lane to the vehicle. Therefore, safety-critical applications, such as an FCW system, know the exact position of the vehicle in a discrete fixed time horizon. To achieve this and to be able to adapt itself to the available resources—sensor output—more accurate models were developed for the vehicle motion, so that the path is estimated even if RBs and lanes are not available to the system. In this paper, the sources of information are taken from the EUCLIDE project; however, the algorithms and the models can be applied using several sources without any loss of generality, e.g., road information from a camera or from map data, obstacles from a stereo vision system, a laser scanner, etc. In the EUCLIDE system, a CW application was developed based on the proposed approach, and the results were evaluated as promising. The authors aim at integrating, testing, and evaluating the path prediction algorithms to other applications such as a lane keeping, lane departure warning, collision mitigation, and safe speed in the near future.

In the future, three research directions are proposed for the improvement of the estimation error. First, more efficient algorithms should be investigated for the "maneuver detection";

tools from evidential reasoning theory (Bayesian, Dempster–Shafer, etc.) give more powerful capabilities in decision systems for the management of uncertain sources of information and could assist the algorithm in assigning the correct model to the path prediction. Second, the inclusion of more input, i.e., more sources of information, will be investigated by the authors without changing the architecture. Finally, the use of an interactive multiple model filter will be investigated. It provides an improved combination of multiple sources of information. Nevertheless, it can lead to increased complexity and workload of the system.

Finally, the method can be applied to the calculation of the path of the other road users, i.e., moving vehicles, pedestrians, cyclists, etc. Although the problem is similar, it needs special attention due to sensor characteristics, e.g., a poor estimation of the lateral attribute of the objects in radar signals.

APPENDIX

In this section, a method that is used to find, in every scan, the true trajectory that the vehicle will follow in the future is described. This trajectory will be used to calculate the rms errors of the predicted values. This method cannot be applied in real-time calculations because it makes use of all the measurements coming from a specific data sequence. First, the whole data sequence is processed using a Kalman filter, and the estimated state of the vehicle, including its velocity V, turn rate ω, and heading θ, is stored in a buffer. Then, the number of the future points of the true trajectory that will be computed is defined, which is usually equal to the number of points that is used to find the future path of the subject vehicle N_p. Then, having the total number N_S of scans contained in the data sequence, the true trajectory at scan k is computed using the following set of equations:

$$\begin{aligned} dx(j|k) &= 0.5 \cdot \omega(j+k-1) \\ &\quad \cdot V(j+k-1) \cdot T^2 \qquad \text{(A.1)} \\ dy(j|k) &= V(j+k-1) \cdot T \\ &\quad + 0.5 \cdot A(j+k-1) \cdot T^2 \qquad \text{(A.2)} \\ \phi(j|k) &= \frac{\pi}{2} - 2 \cdot \theta(j|k) + 2 \cdot \theta(1|k) \qquad \text{(A.3)} \\ g\_dx(j|k) &= dx(j|k) \cdot \sin\left(\phi(j|k)\right) \\ &\quad + dy(j|k) \cdot \cos\left(\phi(j|k)\right) \qquad \text{(A.4)} \\ g\_dy(j|k) &= dy(j|k) \cdot \sin\left(\phi(j|k)\right) \\ &\quad - dx(j|k) \cdot \cos\left(\phi(j|k)\right) \qquad \text{(A.5)} \\ x(j|k) &= \sum_{1}^{j} g\_dx(j|k) \qquad \text{(A.6)} \\ y(j|k) &= \sum_{1}^{j} g\_dy(j|k) \qquad \text{(A.7)} \end{aligned}$$

where $k = 1, 2, \ldots, N_S$, $j = 1, 2, \ldots, n_p$, and $n_p <= N_p - k$. The first two equations compute the displacement of the vehicle in the future scans j using the buffer where the estimated state is saved. The error in the calculations is very small since the prediction for every future scan j is done using the predicted values of the previous scan $j-1$. The model that is used for the position update is selected to be the CA model. Next, the third equation computes the angle between the current coordinate system at scan k of the subject vehicle and the initial coordinate system of it at scan 1. Then, the data that have been computed using the first two equations are transformed in order to refer to the current coordinate system. Finally, the last two equations compute the true trajectory of the subject vehicle. The method described earlier was tested using simulated data in the case of extracting the global trajectory that the vehicle has followed, and there is a deviation of less than 1%.

Finally, the total position rms error at scan k of an estimated trajectory is calculated using the following expression:

$$\text{rms}(k) = \frac{\sum_{i=1}^{N_P} \sqrt{\left(x_E(i) - x_T(i)\right)^2 + \left(y_E(i) - y_T(i)\right)^2}}{N_P} \qquad \text{(A.8)}$$

where $[x_E(i), y_E(i)]$ is the coordinate of the position of the vehicle in the future scan i, which is estimated at scan k, for $i = 1, \ldots, N_P$, and $[x_T(i), y_T(i)]$ is the true position of the vehicle in the future scan i, which is calculated at scan k using the previous method. The x and y position rms errors are calculated using a similar expression:

$$\text{rms}_X(k) = \frac{\sum_{i=1}^{N_P} |x_E(i) - x_T(i)|}{N_P} \qquad \text{(A.9a)}$$

$$\text{rms}_Y(k) = \frac{\sum_{i=1}^{N_P} |y_E(i) - y_T(i)|}{N_P}. \qquad \text{(A.9b)}$$

An alternative method that is used to define the rms error can be used. In this case, the error is calculated for a specific time period of the data sequence, for example, N_{PS} scans, and in fact, it represents the trajectory rms error, which has the following form:

$$\text{rms}\, T(i) = \frac{\sum_{j=1}^{N_{\text{PS}}} \sqrt{\left(x_E(j,i) - x_T(j,i)\right)^2 + \left(y_E(j,i) - y_T(j,i)\right)^2}}{N_{\text{PS}}} \qquad \text{(A.10)}$$

where $[x_E(j,i), y_E(j,i)]$ is the coordinate of the estimated position in the future scan i, which is calculated at scan j, for $i = 1, \ldots, N_P$, $j = 1, \ldots, N_{\text{PS}}$, and $k = 1, \ldots, N_S$. The coordinate $[x_T(j,i), y_T(j,i)]$ is the true position of the vehicle at the future scan i, which is calculated at scan j. The x and y trajectory rms errors are calculated using a similar expression:

$$\text{rms}\, T_X(i) = \frac{\sum_{j=1}^{N_{\text{PS}}} |x_E(j,i) - x_T(j,i)|}{N_{\text{PS}}} \qquad \text{(A.11a)}$$

$$\text{rms}\, T_Y(i) = \frac{\sum_{j=1}^{N_{\text{PS}}} |y_E(j,i) - y_T(j,i)|}{N_{\text{PS}}}. \qquad \text{(A.11b)}$$

REFERENCES

[1] Z. Zotomor and U. Franke, "Sensor fusion for improved vision based lane recognition and object tracking with range finders," in *Proc. IEEE Intell. Transp. Syst. Conf.*, 1997, pp. 595–600.

[2] A. Kirchner and T. Heinrich, "Model based detection of road boundaries with a laser scanner," in *Proc. IEEE Int. Conf. Intell. Veh.*, Stuttgart, Germany, 1998, pp. 93–98.

[3] A. Polychronopoulos, A. Amditis, N. Floudas, and H. Lind, "Integrated object and road borders tracking using 77 GHz automotive radars," *Proc. Inst. Electr. Eng.—Radar, Sonar Navigation*, vol. 151, no. 6, pp. 375–381, Dec. 2004.

[4] B. Fardi and G. Wanielik, "Hough transformation based approach for road border detection in infrared images," in *Proc. IEEE Intell. Veh. Symp.*, 2004, pp. 549–554.

[5] NHTSA, "Automotive collision avoidance system field operational test," *ACAS/FOT 3rd Annual Rep.*, May 2003.

[6] D. Swartz, "Clothoid road geometry unsuitable for sensor fusion," in *Proc. IEEE Intell. Veh. Symp.*, Columbus, OH, 2003, pp. 484–488.

[7] Y. Bar-Shalom, X. Rong Li, and T. Kirubarajan, *Estimation With Applications to Tracking and Navigation*. Hoboken, NJ: Wiley, 2001.

[8] X. Rong Li and V. Jilkov, "Survey of maneuvering target tracking," *IEEE Trans. Aerosp. Electron. Syst.*, vol. 39, no. 4, pp. 1333–1364, Oct. 2003.

[9] S. Blackman and R. Popoli, *Design and Analysis of Modern Tracking Systems*. Norwood, MA: Artech House, 1999.

[10] L. Andreone, F. Tango, U. Scheunert, H. Cramer, G. Wanielik, A. Amditis, and A. Polychronopoulos, "A new driving supporting system, integrating an infrared camera and an anti-collision micro-wave radar: The EUCLIDE project," in *Proc. IEEE Intell. Veh. Symp.*, Versailles, France, 2002, pp. 519–526.

[11] U. Scheunert, H. Cramer, A. Polychronopoulos, A. Amditis, G. Wanielik, and L. Andreone, "Multi sensor data fusion for object detection: Challenges and benefit," *J. Ingegneria Automotoristica*, vol. 55, no. 9/10, pp. 301–309, Sep. 2002.

[12] M. Tsogas, A. Polychronopoulos, and A. Amditis, "Unscented Kalman filter design for curvilinear motion models suitable for automotive safety applications," in *Proc. 8th Int. Conf. Inf. Fusion*, Philadelphia, PA, Jul. 25–29, 2005.

Aris Polychronopoulos (M'05) received the degree from the Department of Electrical and Computer Engineering, National Technical University of Athens (NTUA), Athens, Greece, on July 2000 and the Ph.D. degree on motion modeling and tracking techniques in automotive active safety applications from the Microwaves Laboratory of DECE, NTUA.

He was a teaching assistant for the undergraduate and graduate courses on microwaves and was a Lecturer for a seminar on multitarget multisensor data fusion. His research interests include radar systems design, remote monitoring applications, and communication theory. He has experience both on European and national projects.

Manolis Tsogas received the Diploma in electrical and computer engineering from the National Technical University of Athens (NTUA), Athens, Greece, in 1992, where he is currently working toward the Ph.D. degree with the Microwaves Laboratory of DECE.

Angelos J. Amditis (M'03) received the Diploma degree in electrical and computer engineering and the Ph.D. degree in electrical and computer engineering (telecommunications) from the National Technical University of Athens (NTUA), Athens, Greece, in 1992 and 1997, respectively.

He has been teaching various courses (communication and computer networks, communication theory, etc.) at the Department of Electrical and Computer Engineering and Institute of Communications and Computer Systems (ICCS), NTUA, and the Hellenic Naval Academy for the last five years. He is a Research Assistant Professor and a Project Manager with the Microwaves and Fiber Optics Laboratory, ICCS, NTUA. He is the author of several conference papers and of a Greek high school-level book about telecommunication and networks. His current research interests are in the fields of human–machine interfaces, telematics, data security, computer networks, Internet, Intranets, software development, virtual reality, telecommunications systems, electromagnetic compatibility/electromagnetic interference (EMC/EMI), radars, etc.

Luisa Andreone started in 1990 with the development of different measurement systems for vehicle production lines, climate and EMC test chambers, and ergonomic measurements. Her expertise includes several years of experience in managing a number of national and international projects (e.g., DARWIN, EUCLIDE, and EDEL), as well as projects within the Fiat Group. At Fiat Research Centre, Torino, Italy, she is a Project Manager who is responsible for the international activities within the Electro-Telematic Systems Department. Within the initiatives of the Sixth Framework Program, she is a member of the Core Groups of the Adaptive Integrated Driver-vehicle InterfacE (AIDE) and of the Towards Global System for Telematics-Integrated Projects (GST-IPs) and industrial leader of the AIDE technological subproject. Since January 2007, she has been the Leader of the EUCAR Working Group SGI human–vehicle interaction. While she was with the PROMETHEUS project, she was a European Function Coordinator of the CED1 "Vision Enhancement." She is responsible for the development of different demonstrator vehicles that are integrating different driving support systems and innovative human–machine interfaces.